Title

β-catenin mRNA encapsulated in SM-102 lipid nanoparticles enhances bone formation in a murine tibia fracture repair model.

Authors

Nelson, Anna
Mancino, Chiara
Gao, Xueqin
et al.

Publication Date

2024-09-01

DOI

10.1016/j.bioactmat.2024.05.020

Peer reviewed

Bioactive Materials 39 (2024) 273–286

Contents lists available at ScienceDirect

Bioactive Materials

journal homepage: www.keaipublishing.com/en/journals/bioactive-materials

β-catenin mRNA encapsulated in SM-102 lipid nanoparticles enhances bone formation in a murine tibia fracture repair model

Anna Laura Nelson [a,d,1], Chiara Mancino [b,1], Xueqin Gao [a], Joshua A. Choe [c], Laura Chubb [e], Katherine Williams [f], Molly Czachor [a], Ralph Marcucio [h], Francesca Taraballi [b], John P. Cooke [g], Johnny Huard [a,e], Chelsea Bahney [a,e,h,**], Nicole Ehrhart [d,e,f,*]

[a] Steadman Philippon Research Institute (SPRI), Center for Regenerative and Personalized Medicine, Vail, CO, USA
[b] Houston Methodist Research Institute, Center for Musculoskeletal Regeneration, Houston TX, USA
[c] University of Wisconsin-Madison, Department of Orthopedics and Rehabilitation, Department of Biomedical Engineering, Medical Scientist Training Program, Madison, WI, USA
[d] Colorado State University, School of Biomedical Engineering, Fort Collins CO, USA
[e] Colorado State University, Department of Clinical Sciences, Fort Collins CO, USA
[f] Colorado State University, Department of Microbiology, Immunology, and Pathology, Fort Collins, CO, USA
[g] Houston Methodist Research Institute, Center for RNA Therapeutics, Department of Cardiovascular Sciences, Houston, TX, USA
[h] University of California, San Francisco (UCSF), Orthopaedic Trauma Institute, San Francisco, CA, USA

ARTICLE INFO

Keywords:
Gene therapy
Fracture healing
Lipid nanoparticles
mRNA
Canonical Wnt

ABSTRACT

Fractures continue to be a global economic burden as there are currently no osteoanabolic drugs approved to accelerate fracture healing. In this study, we aimed to develop an osteoanabolic therapy which activates the Wnt/β-catenin pathway, a molecular driver of endochondral ossification. We hypothesize that using an mRNA-based therapeutic encoding β-catenin could promote cartilage to bone transformation formation by activating the canonical Wnt signaling pathway in chondrocytes. To optimize a delivery platform built on recent advancements in liposomal technologies, two FDA-approved ionizable phospholipids, DLin-MC3-DMA (MC3) and SM-102, were used to fabricate unique ionizable lipid nanoparticle (LNP) formulations and then tested for transfection efficacy both *in vitro* and in a murine tibia fracture model. Using firefly luciferase mRNA as a reporter gene to track and quantify transfection, SM-102 LNPs showed enhanced transfection efficacy *in vitro* and prolonged transfection, minimal fracture interference and no localized inflammatory response *in vivo* over MC3 LNPs. The generated β-catenin^{GOF} mRNA encapsulated in SM-102 LNPs (SM-102-β-catenin^{GOF} mRNA) showed bioactivity *in vitro* through upregulation of downstream canonical Wnt genes, *axin2* and *runx2*. When testing SM-102-β-catenin^{GOF} mRNA therapeutic in a murine tibia fracture model, histomorphometric analysis showed increased bone and decreased cartilage composition with the 45 μg concentration at 2 weeks post-fracture. μCT testing confirmed that SM-102-β-catenin^{GOF} mRNA promoted bone formation *in vivo*, revealing significantly more bone volume over total volume in the 45 μg group. Thus, we generated a novel mRNA-based therapeutic encoding a β-catenin mRNA and optimized an SM-102-based LNP to maximize transfection efficacy with a localized delivery.

1. Introduction

Fractures continue to be one of the most frequent type of hospitalized traumas with reports of about 32.7 million new cases of lower leg fractures globally in 2019 [1,2]. The most frequent fracture amongst long bones is tibial shaft fractures, and despite surgical interventions upwards of 15–48 % of patients with this type of fracture fail to heal as expected [3–7]. The risk of developing impaired fracture healing (non-union or delayed union) is often highest in patients with open tibial fractures or medical co-morbidities with tibial non-union having a more

Peer review under responsibility of KeAi Communications Co., Ltd.
* Corresponding author. Colorado State University, Department of Clinical Sciences, Fort Collins CO, USA.
** Corresponding author. Colorado State University, Department of Clinical Sciences, Fort Collins CO, USA.
E-mail addresses: cbahney@sprivail.org (C. Bahney), nicole.ehrhart@colostate.edu (N. Ehrhart).
[1] Co-first author.

https://doi.org/10.1016/j.bioactmat.2024.05.020
Received 29 December 2023; Received in revised form 8 May 2024; Accepted 8 May 2024

significant impact on patient quality of life than congestive heart failure or myocardial infarction [6,8]. Over the last decade, significant advancements in the molecular and cellular understanding of fracture healing have led to new mechanisms that may be capitalized upon in the quest for novel therapeutic targets to promote repair [9–12].

Fractures heal through a tightly regulated process consisting of overlapping, yet distinct sequences of essential repair steps [10]. The first stage consists of a robust inflammatory response, involving the secretion of cytokines and growth factors imperative in the recruitment of progenitor cells, cells necessary in driving osteoblastogenesis [10,13]. Bone forms through two distinct mechanisms: direct and indirect bone formation [14]. Direct bone formation, or intramembranous ossification, involves the direct differentiation of progenitor cells to osteoblasts [14]. Indirect bone formation, or endochondral ossification, involves progenitor cells differentiating into a cartilage intermediate prior to transdifferentiating into osteoprogenitors and osteoblasts [14–18]. The final remodeling stage involves the replacement of trabecular bone with cortical bone [10]. Aberrations within any of these fracture healing stages can lead to delays or impairments in fracture repair [10]. Other than additional surgery, biologic solutions to facilitate fracture healing in non-union or delayed union cases are limited. The only FDA-approved osteoanabolic, recombinant human bone morphogenetic protein-2 (BMP-2), has limited use in the clinic and is currently only approved for specific spinal fusion cases and acute, open tibial shaft fractures. Its clinical success has been limited by significant adverse reactions, such as heterotopic ossification [19–24]. As such, these clinical side effects have prompted the exploration of other therapies with fewer untoward consequences. There remains a clinical need to develop safe and effective therapies for the stimulation of bone in fracture repair.

Mechanistic data highlighting the necessity of canonical Wnt pathway during fracture repair has facilitated a framework for Wnt-based therapeutics [10,11]. β-catenin was found to regulate chondrocyte-to-osteoblast transdifferentiation during fracture repair as detected through genetic deletion and stabilization of Wnt in a murine model [18]. Therapies aiming to directly activate Wnt have been met with manufacturing and delivery challenges due to the insoluble characteristics of lipidated Wnt ligands [25,26]. Current clinical approaches involve the indirect activation of the canonical Wnt pathway through targeting the inhibitors of Wnt, such as Sclerostin [26,27]. Preclinical success using indirect approaches was reported in osteoporosis applications, yet these indirect strategies were not found to be efficacious in fracture repair [28]. The use of RNA therapy to directly activate the canonical Wnt pathway would likely mitigate the limitations associated with the production of hydrophobic Wnt proteins. Despite these overcoming these challenges, RNA therapeutics continue to be limited by stability of the RNA transcript and stimulating an innate immune reaction.

Recently, there have been significant advancements in lipid-based nanotechnology for nucleic acid and drug delivery, which have resulted in the successful clinical translation of several novel and highly effective therapies [29]. Specifically, optimization of physiochemical properties like particle size, surface charge, and long-term stability have promoted successful clinical translation [30]. The most recent breakthrough in this field are carriers known as lipid nanoparticles (LNPs), nanosized vesicles that ensure RNA encapsulation in the protected core due to the physio-chemical properties of all components [31]. LNPs have been successfully translated to the clinic in several instances, such as with the Onpattro® formulation, used to deliver small interfering RNA for the treatment of transthyretin amyloidosis, or with the Pfizer-BioNTech (BNT162b2) and Moderna (mRNA-1273) formulations, that achieved outstanding protection against the SARS-CoV-2 virus. The key components of all the aforementioned lipid-based delivery system include: (i) an ionizable cationic lipid, (ii) a helper lipid known as DSPC (1,2-distearoyl-sn-glycero-3-phosphocholine), (iii) cholesterol, and (iv) a pegylated lipid [32]. All four components have specific roles in both the encapsulation and the delivery process. A central feature of ionizable LNPs that gives rise to high transfection capacity is a formulation parameter known as "apparent pK_a", ideally between 6 and 7, which enhances endosomal escape of the mRNA through electrostatic interaction of the endosomal phospholipids and cationic ionizable lipids [54,55].

In this study, our goal was to develop and test an mRNA construct encoding a β-catenin sequence, β-catenin^{GOF}, for stimulating bone regeneration by activating the canonical Wnt signaling pathway at a temporally optimized time within bone repair. We hypothesized that delivery of a chemically modified β-catenin^{GOF} mRNA encapsulated in SM-102 LNPs would activate the canonical Wnt pathway and promote endochondral bone formation. We investigated two lipidic compositions in the fabrication of LNPs for mRNA delivery in a fracture repair application. Here, we tested a more traditional ionizable lipid composition, MC3 LNP, against a modified version of the Moderna ionizable LNP formulation, SM-102 LNP. Validation of the bioactivity and efficacy of SM-102-β-catenin^{GOF} mRNA in promoting bone were performed *in vitro* and *in vivo* following a localized delivery to the fracture site in a murine tibia fracture model. The therapeutic developed in this study has the potential to mitigate additional surgeries required to intervene for impaired fracture healing cases.

2. Materials & Methods

2.1. Lipid nanoparticle synthesis and characterization

Two different ionizable lipid nanoparticles (LNPs) were formulated for use in the following experiments to determine the most favorable formulation to deliver mRNA to the fracture callus. Lipid nanoparticles containing mRNA were synthesized with the microfluidic system Benchtop Nanoassemblr. Ionizable lipids DLin-MC3-DMA (MC3) and SM-102 were purchased from MedChemExpress (Cat # HY-112251, HY-134541 respectively). Cholesterol (Cat # 700000P), 18:0 DSPC (Cat # 850365P) 18:1 (Δ9-Cis) PC DOPC (Cat # 850375P), and DMG-PEG2000 (Cat # 880151P) were purchased from Avanti Polar Lipids. First, 300 μg of mRNA was dissolved in 750 μl of sodium citrate buffer (150 mM, pH = 4.5) to make up the aqueous phase, while the lipids DLin-MC3-DMA: DSPC:Cholesterol:DMG-PEG2000 (MC3), and the lipids SM-102:DOPC: Cholesterol:DMG-PEG2000 (molar ratios 50:10.5:38:1.5) (SM102) were dissolved in 250 μl of ethanol to make up the organic phase. Second, both of the phases were warmed to 45 °C and loaded into syringes for synthesis using the Nanoassemblr microfluidic device using pre-set parameters (flow rate ratio = 1:3 (organic:aqueous), total flow rate = 9 ml/min, waste = 100 μl). The final N/P ratio (ratio between the positively charged amine groups from the ionizable lipids over the negatively charged phosphate groups from the mRNA) was set to 6 independently of the mRNA sequence. After synthesis, LNPs were dialyzed against 1x PBS (overnight, 4 °C) and filtered with 0.22 μm syringe filters.

Physio-chemical properties of each LNP formulation were measured via dynamic light scattering (DLS, Malvern Zetasizer), for up to 4 weeks upon storage at 4 °C. To measure size and polydispersity index, 10 μl of LNPs were diluted in 990 μl of PBS and Zeta potential (mV) measurements were collected using a solution containing 10 μl LNPs, 90 μl PBS and 900 μl of double distilled water. In all cases, the equipment was set to average three sets of measurements with 15 sub-runs each. mRNA encapsulation efficiency (EE%) was measured using the Ribogreen RNA assay (Invitrogen, Cat #R11490). First, LNPs were initially diluted 1:100 in TE buffer and then subsequently diluted 1:2 in either TE buffer (to measure un-encapsulated RNA), or 2 % (v/v) Triton-X in TE buffer (to lyse LNPs and measure encapsulated RNA), for a total volume of 100 μl. The diluted LNPs were incubated for 15-min at 37 °C. Ribogreen reagent was diluted 1:10 in TE buffer and 100 μl were added to the diluted LNPs. Following a 10-min incubation at room temperature, the plate was read at Ex/Em of 480nm/520 nm. Results obtained from LNPs diluted in TE buffer were subtracted from those obtained for LNPs diluted in Triton-X

to calculate the final mRNA concentration.

Two mRNA sequences were used to execute all *in vitro* and *in vivo* assays, firefly luciferase and a non-destructive β-catenin sequence, β-catenin^{GOF}. Firefly Luciferase mRNA (TriLink Biotechnologies, Cat #L7202) was used as a reporter gene. β-catenin^{GOF} sequence was developed based on gain-of-function phenotypes that have been previously published [33]. The sequence was then optimized using online codon optimality tool, icodon.org. N1-methyl-pseudouridine was used as a modified nucleoside to replace all uridines and Clean Cap technology was used as a 5' cap. The mRNA construct was generated at the RNA Core facility at Houston Methodist. The RNA Core facility uses proprietary untranslated regions (UTRs) and additionally a long poly A tail of 151 bases. The generated β-catenin^{GOF} mRNA was encapsulated using SM-102 LNPs as detailed in the lipid nanoparticle synthesis methodology.

2.2. Testing transfection efficacy and cytotoxicity in vitro

hMSCs were grown in alphaMEM (VWR, Cat # 50-012-PC) supplemented with 10 % FBS (Gibco, Cat # 16000-044) and 1 % Penicillin/Streptomycin (Hyclone, VWR, Cat # SV30010). mRNA and LNPs were diluted in OptiMEM (Gibco, Cat # 11058021), delivered at 100 ng mRNA/well to human BM-MSCs and incubated overnight, $n = 3$. Cells were treated for 24 h and then were washed with PBS 2X and lysed (5:1 PBS to CCLR) (Promega, Cat #E1531). Firefly Luciferase activity was assayed by mixing Firefly luciferase assay buffer (50 mM Tris, 10 mM MgSO4, 6 mM D/L cysteine, 20 μM Sodium Pyrophosphate, 1 mM EDTA and 2 g/L Bovine serum album) with ATP (1 mM Final), and D-Luciferin (150 μg/mL). 100 μL of this assay buffer was added to 20 μL of lysate and read on a plate reader for bioluminescence.

The CellTiter-Blue® Reagent was employed to measure cytotoxicity of hMSCs as the ingredients have been optimized for use to study cell viability. The spectral properties of CellTiter-Blue® Reagent change upon reduction of resazurin to resorufin. Resazurin is dark blue in color and has little intrinsic fluorescence until it is reduced to resorufin, which is pink and highly fluorescent. Celltiter Blue Reagent (Promega, Cat #G8080) was mixed 1:5 with cell culture media and incubated for 1 h with cells, $n = 3$. The plate was then read at 579Ex/584 Em. Basal media with Celltiter Blue Reagent was used to control background signal and metabolic activity was compared between the treated and untreated groups.

2.3. Testing bioactivity of β-catenin^{GOF} mRNA in vitro

To test bioactivity of β-catenin^{GOF} mRNA, β-catenin^{GOF} mRNA encapsulated in SM-102 LNPs was delivered to hypertrophic ATDC5 cells. For all *in vitro* experiments, ATDC5 cells were plated in triplicate at 20,000 cells/well in 12 well plates, $n = 3$. Passage 5 and under was used for all *in vitro* experiments. ATDC5 cells were maintained using basal medium DMEM/F12 (Thermo Fisher, Cat# 11320033), 5 % fetal bovine serum (FBS, Thermo Fisher, Cat# 16000044) and 1 % penicillin/streptomycin (P/S, Thermo Fisher, Cat# 15140122) until hypertrophic differentiation. ATDC5 cells were then differentiated into hypertrophic chondrocytes over a series of 7 days. Hypertrophic chondrocyte differentiation involved use of basal ATDC5 medium supplemented with 1 % L-Glutamine (ThermoFisher, Cat # 25030149), 10 μg/mL transferrin (Millipore Sigma, Cat #T8158-100 mg), 3×10^{-8} M Selenite (Sigma Aldrich, Cat #S5261-10G), 0.2 mM Ascorbic Acid (Sigma Aldrich, Cat # A8960-5G), and 10 μg/mL Insulin (Millipore Sigma, Cat #I2643-25 MG) treated on cells for 7 days with replacing media every 2–3 days. [34]). Prior to transfection experiments, chondrocytes underwent serum starvation using basal media OPTI-MEM (Thermo Fisher, Cat# 31985070), 0.5 % FBS and 1 % P/S for 24 h. Transfection was performed using serum-free media, OPTI-MEM supplemented with 1 % P/S, delivered at a concentration involved 0.25 μg mRNA/well, 100 ng/mL rhWnt3a (R&D Systems, Cat # 5036-WN-010) for the positive control, and serum-free media as the negative control [35–37]. Following transfection for 6 h, RNA was isolated from each well, made into cDNA and qRT-PCR was performed for downstream genes from canonical Wnt, *axin2* and *runx2,* to evaluate Wnt activation. Canonical Wnt activation was measured using experiments including Topflash assay and qRT-PCR for *axin2* and *runx2*.

Topflash was used to measure *in vitro* bioactivity of β-catenin mRNA using a reporter plasmid assay. Topflash (M50) vector contains a promoter region coupled to Tcf-binding sites with an upstream firefly luciferase gene. The plasmid vectors were co-transfected with Renilla luciferase plasmids as a control for transfection efficacy. First, plasmid vectors M50 (Addgene, Cat # 12456), M51 (Addgene, Cat # 12457) and Renilla (Addgene, Cat # 27163) were grown on amp-resistant agar plates (Thermo Fisher, Cat #J63197EQF) overnight at 37 °C. A single colony was then amplified in liquid amp-resistant LB broth overnight at 37 °C. Plasmids were then isolated using ZymoPure II Plasmid Maxiprep Kit (Zymo Research, Cat #D4202) according to manufacturer's instructions. ATDC5 cells were transfected with plasmid vectors using Lipofectamine 3000 according to manufacturer's instructions, delivering a total of 10 μL total solution/well and delivering 1 μg of pDNA/well, $n = 3$. Renilla was used at 1/10th the concentration of M50 and M51. The plasmids were transfected for 2 days prior to treating with 100 ng/mL rhWnt3a, as the positive control, or with 2 μg/well β-catenin mRNA. Lipofectamine MessengerMax was used to deliver mRNA according to manufacturer's instructions. Treatments were incubated for 48 h prior to analysis. Firefly/Renilla Dual Luciferase Assay (Sigma Aldrich, Cat # SCT152) was used as a reporter assay to quantify both firefly and renilla luciferase expression and was used per manufacturer's protocol. Topflash results were reported as a ratio of Firefly to Renilla signal [38,39].

2.4. Tibia fracture repair model

In vivo experiments were approved by and conducted in compliance with the Institutional Animal Care and Use Committee at Colorado State University (CSU). Mice were socially housed throughout the in-life period and permitted free ambulation. Mid-shaft tibial fractures were created in adult (12–14 weeks), male C57BL/6J mice (Charles River # 027). (Describe treatment groups and numbers here) All animals received a pre-surgical analgesic, Buprenorphine SR (ZooPharm), at a dose of 0.6–1.0 mg/kg. Mice were placed under general anesthesia using inhaled 1–5 % isoflurane to effect. Left hind limbs were shaved and sterilely prepared using 70 % alcohol wipes and Chlorhexidine surgical scrub solution, repeated for a total of 3 times. Lubrication was provided for the eyes of each mouse using artificial tears ointment (Bausch & Lomb) and mice were then transferred to a heated operating table. Using aseptic technique, an incision was made along the tibia, and a hole was made at the top of the tibial plateau using a 23-gauge needle. An intermedullary pin (sterilized insect pin) was inserted through the hole made from the tibial plateau through the tibial cavity and into the distal tibia. One small hole was created in the mid-shaft of the tibia using a Dremel and pressure was applied to both proximal and distal ends to create a pin-stabilized tibia fracture. The surgical incision was then sutured using 5-0 Biosyn Sutures (Covidien, Cat #5687) and one surgical skin staple was applied over the skin incision to protect against chewing. A local anesthetic, 0.25 % Bupivacaine Hydrochloride (NovaPlus, cat # RL-7562), was applied topically after the initial staple was placed. Mice were closely monitored for proper ambulation on the surgical limb and signs of infections for 72 h following the surgery. If any signs of aberrant ambulation were observed, these mice were injected with an additional round of Buprenorphine SR at a dose of 0.6–1.0 mg/kg, as recommended and under supervision from veterinary staff. All treatments were injected locally to the site of the fracture callus 6 days following fracture based on our prior work demonstrating genetic overexpression of β-catenin/canonical Wnt from day 6 to day 10 post-fracture accelerated fracture repair [40]. To determine the ability of ionizable MC3 and

SM-102 LNPs to deliver mRNA, MC3 and SM102 LNPs were concentrated to allow for a 25 μL injection volume using 100K protein concentrators (Sigma Aldrich, Cat # UFC510024), spun at 5000×*g* for 5–10 min (*n = 5/group*). Firefly luciferase (FLuc) mRNA was used as a reporter gene at 10 μg/mouse. Negative control groups included a sterile-filtered phosphate buffered saline (PBS) group. To determine β-catenin^{GOF} mRNA bioactivity *in vivo*, SM-102-β-catenin^{GOF} mRNA was concentrated to allow for a 25–30 μL injection volume/mouse using 100K protein concentrators spun at 5000×*g* for 5–10 min. SM-102-β-catenin^{GOF} mRNA was delivered at concentrations of 10, 25 and 45 μg/mouse (*n = 6-10/group*). The negative control group was sterile-filtered phosphate buffered saline (PBS) group. Positive control was rhWnt3a (R&D Systems, Cat # 5036-WN-010), at a concentration of 1 μg/mL at similar volume [41,42]. All treatments were vortexed for 10 s prior to aspirating into the Hamilton 1800 series syringe (Hamilton, Cat # 84881) and were then injected locally to the fracture callus. Animals were sacrificed according to approved euthanasia protocols.

2.5. Transfection efficacy and kinetics testing in vivo

Transfection efficacy and kinetics were measured using firefly luciferase mRNA and protein expression was quantified using IVIS bioluminescence imaging. IVIS imaging was performed at 24 h and every day following injection until signal dissipated. IVIS imaging was performed daily to quantitatively assess the magnitude and duration of luciferase expression from the time of delivery of reporter mRNA, *n = 3-5*. All mice were anesthetized using isoflurane and injected with 100 μL of firefly luciferase substrate, D-luciferin, subcutaneously at 30 mg/mL in PBS. Continued isoflurane was maintained at 1–5% and mice were imaged 5 min following subcutaneous injection of D-luciferin. Bioluminescence was acquired using the 'Auto' setting and regions of interest were measured for bioluminescence using LivingImage software. To assess the biodistribution following localized injections of the LNP-mRNA therapies, IVIS imaging was performed at 6 and 18 h following treatments. To acquire ex-vivo IVIS images, mice were sacrificed according to approved euthanasia protocols after 18 h following localized treatments. Immediately following live IVIS imaging, fractured limb, liver, lung, spleen and kidney were harvested and imaged *ex-vivo*. Bioluminescence was acquired using the 'Auto' setting and regions of interest were measured for bioluminescence using LivingImage software. All tissues were then flash frozen immediately using liquid nitrogen and stored at −80 °C.

2.6. In vivo immunogenicity and fracture healing interference measurements

To further examine the immunogenic and osteogenic effects after delivering MC3 and SM-102 LNPs, qRT-PCR was performed on various markers, *n = 3-5*. To isolate RNA from the fracture callus, the tissue was dissected, minced into small pieces and placed in 1 mL of TRIzol. The tissues were then homogenized using IKA Tissue Homogenizer (IKA, Cat# 0003737001) using a speed of 5 for 3 min, or at least until all large chunks were broken down. RNA was isolated using TRIzol™ Reagent (ThermoFisher, Cat# 15596026) according to the manufacturer's guidelines. RNA was then quantified by reading the absorbance values at 260 and 280 nm. 1 μg of RNA was then synthesized into cDNA using qScript cDNA SuperMix (QuantaBio, Cat# 95048-025). Next, primers were designed and are listed in Table 1. Quality measurements were used to confirm primer specificity and appropriate reaction temperatures by running PCR using DreamTaq Green PCR Master Mix (2X) (ThermoFisher, Cat# K1081) using a 3-step method with denaturation at 95 °C for 30 s, annealing at 60 °C for 30 s and extension at 72 °C for 1 min. The bands were analyzed on a 1.5 % agarose gel with 2 μL GelStar Nucleic Acid Stain (Lonza, Cat # 50535) run at 150V for 25 min. Quantitative real-time PCR was run using SYBR Green Master Mix (Bio-Rad, Cat#1725270) to detect the amplified DNA. qRT-PCR was performed on a StepOnePlus™ instrument (Applied Biosystems). To analyze the output Ct values, the reference housekeeping gene (β-2-modulin) was used to determine ΔCt values. The value of 2-(ΔΔCt) was calculated for all graphs and to determine statistical significance. All 2 (-ΔΔCt) values less than 1.0, were calculated as −1/(2(-ΔΔCt)) as followed and described in Schmittgen et al. [34] Local inflammatory response was measured using qRT-PCR while systemic inflammation was tested using a C-Reactive Protein (CRP) ELISA kit (R&D Systems, Cat# MCRP00) according to manufacturer's instructions on the serum collected at day 1 and 10 post-treatment, *n = 3-5* [43].

2.7. Histology and histomorphometry

Fractured tibias of treated mice were collected 2 and 8 days post injection, immersion fixed in 4 % paraformaldehyde, and decalcified using 19 % ethylenediaminetetraacetic acid (EDTA), *n = 6-8*. The tissues were then processed in increased ethanol solutions (50 %, 70 %, 95 % and 100 %), processed in xylene (x2) and then placed in paraffin for 1.5 h each. Samples were embedded in paraffin, sectioned at 8 μm thickness, and mounted onto glass slides. To perform quantitative histomorphometry, serial sections were obtained using the first section beginning in the fracture callus and every 10th section afterwards. Standard histomorphometry principles were used and quantification of the fracture callus components including bone, cartilage and fibrous tissues were determined [15,44]. Hall Brundt Quadruple stain was used to identify the dense collagenous fibrils of bone, stained red by direct red, and proteoglycans in the cartilage matrix, stained by alcian blue [45]. Quantification of callus composition was determined using the Trainable Weka Segmentation2 add-on in Fiji ImageJ (version 1.54f; NIH, Maryland, USA) and was trained to detect bone, cartilage, fibrous tissues and background [46]. Volume of specific tissue types was determined by summing the individual compositions relative to the whole fracture callus compositions. Tissues were imaged using a Nikon Eclipse Ti microscope. Additionally, photoshop (version 24.7.0, Adobe) was used to isolate fractured tissue from the adjacent muscle and skin tissues.

2.8. μCT analysis

Mice were sacrificed at 2 weeks following fracture and stabilization and the fractured tibia was dissected and fixed in 4 % paraformaldehyde (PFA). MicroCT and microCT analysis was performed as previously

Table 1
Primer sequences validated for use in qRT-PCR for use in all LNP treated fracture calluses.

Gene	Forward	Reverse
β-2-modulin	ATACGCCTGCAGAGTTAAGCA	TCACATGTCTCGATCCCAGT
Collagen 10a1 (col10a1)	TTCTGCTGCTAATGTTCTTGACC	GGGATGAAGTATTGTGTCTTGGG
Alkaline Phosphatase (alp)	GTTGCCAAGCTGGGAAGAACAC	CCCACCCCGCTATTCCAAAC
interleukin-1β (il-1β)	TGGACCTTCCAGGATGAGGACA	GTTCATCTCGGAGCCTGTAGTG
Tumor necrosis factor- α (tnf α)	GGTGCCTATGTCTCAGCCTCTT	GCCATAGAACTGATGAGAGGGAG
firefly luciferase (fluc)	GTGGTGTGCAGCGAGAATAG	CGCTCGTTGTAGATGTCGTTAG
axin2	GTGAGCTGGTTGTCACCTACTT	GCAAATTCGTCACTCGCCTTC
runt-related transcription factor 2 (runx2)	ACTCTTCTGGAGCCGTTTATG	GTGAATCTGGCCATGTTTGTG

published, $n = 7\text{-}10$ [47,48]. Briefly, fixed bones were scanned using MicroCT (Viva CT-80, Scanco Medical, Switzerland) at 15 μm resolution, 70 kVP and 112 μA X-ray energy. Bone volume was quantified using Scanco evaluation software according to the guidelines of the American Society of Bone and Mineral Research (ASBMR). The mid-point of fracture callus was selected, and 150 slices above and below were analyzed for a total of 300 slices to be evaluated per mouse. Trabecular bone quantity was analyzed with a Gauss = 0.8, Sigma = 1, threshold of 184. Bone volume, total volume, trabecular number, trabecular separation, trabecular thickness, connectivity density, structure model index, and volumetric bone density were all CT parameters.

2.9. Immunohistochemistry

Immunohistochemical staining for β-catenin (β-CAT) was performed using a similar protocol as previously described, $n = 5\text{-}6$ [49–51]. Briefly, paraffin sections were deparaffinized and rehydrated in water. Heat-mediated antigen retrieval was performed using sodium citrate buffer (10 mM, pH = 6.0) for 20 min in a water bath at 91 °C and cooled for 10 min. All sides were washed in PBS three times and then blocked with 5 % donkey serum (017-000-121, Jackson ImmunoResearch) in PBS for 1 h. The section slides were then incubated in rabbit-anti-β-CAT primary non-phosphorylated antibody (ab 223075, 1:1000 dilution, Abcam, Waltham, MA, USA) in a 5 % donkey serum/PBS solution at 4 °C overnight. The slides were then washed with PBS three times and treated with 0.5 % hydrogen peroxide in PBS for 30 min at ambient temperature. After another three PBS washes, slides were then incubated with a biotinylated horse anti-rabbit-IgG (BA-1100-1.5, Vector Laboratories Inc., Newark, CA, USA) at a 1:300 dilution. After another three PBS washes, the slides were then incubated with VECTASTAIN® Elite ABC-HRP Kit (Peroxidase, Universal) (Vector Laboratories Inc., Newark, CA, USA) for another 2 h according to manufacturer's protocol. After PBS wash, a DAB kit (SK-4100, Vector Laboratories Inc., Newark, CA, USA) was used for color reaction to reveal positive cells. After rinsing with water, Hematoxylin QS (H-3404-100, Vector Laboratories Inc., Newark, CA, USA) was used to counterstain the cell nuclei. Slides were then dehydrated in gradient alcohol, cleared with xylene, dried, and a coverslip was then applied with Acrymount Mounting Medium (IHC World, LLC, Ellicott City, MD). Images were captured with a Nikon NI microscope (Nikon Instruments Inc., Melville, NY, USA). Positive cell numbers and bone surface or area were counted and measured using Image J software. Positive cells were stained brown. Activated β-CAT located in the cell nuclei. Inactivated phosphorylated β-CAT located at cytoplasm or membrane. The positive cells were expressed as cell number/mm bone surface or cell number/mm bone area.

2.10. Statistics

Animal sample size was determined *a priori* using the mean and standard deviation from our preliminary data, where a power analysis was conducted using RStudio to determine that 7 mice/group/time are required for histomorphometry analysis to achieve a power level >80 % with an effect size d = 0.24 and a significance level of 5 %. Moreover, a significance level of 5 % was chosen for all studies. Statistical analysis was performed using Graph Pad Prism 8. All data were plotted so that each sample represented a single point on each graph. Each bar indicates the mean with error bars representing standard deviation. Statistical difference was determined by ANOVAs and all post-hoc comparison performed using Tukey's HSD test.

3. Results

3.1. SM-102 LNPs improved mRNA delivery as compared with MC3 LNPs in vitro

SM-102 and MC3 LNPs were generated and then characterized to determine differences between the two formulations. First, we characterized the LNPs through size, polydispersity index (PDI) and surface charge (Fig. 1A). MC3 and SM-102 LNPs were of similar size, with MC3 LNPs being 101.04 ± 1.97 nm and SM-102 LNPs being 105.0 ± 0.73 nm. PDI reveals a monodisperse LNP sample set, as both are under a PDI of 0.15 (0.11 ± 0.01 a.u. for MC3 LNPs, and 0.09 ± 0.01 a.u. For SM-102 LNPs) [52]. Additionally, the Zeta potential, or the surface charge of nanoparticles in solution, analysis resulted in near net neutral surface charges for both of the LNPs (−5.55 ± 1.01 mV for MC3 LNPs, and −5.57 ± 0.30 mV for SM-102 LNPs), according to literature guidleines that describe net neutral nanoparticles fall within the range of −10 and + 10 mV, while cationic and anionic nanoparticles are characterized as having a surface charge of ±30 mV and over/under [53]. Finally, while the encapsulation efficiency of the MC3 formulation has been characterized by our group elsewhere, SM-102 formulation displayed an encapsulation efficiency of over 85 % [54]. As shown in SUPPLEMENTARY Fig. 1, both physio-chemical properties and encapsulation efficiency remained consistent for four weeks upon storage at 4C, $n = 3$.

Transfection efficacy was assessed in human bone-marrow MSCs using firefly luciferase as a reporter gene to track and measure level of transfection following delivery with 0.5 μg mRNA/well, $n = 3$. A one-way ANOVA showed significance between luminescence and treatment groups, $F(2,6) = 149.8$, $p < 0.0001$. SM-102 significantly increased transfection compared to MC3 LNPs and the no treatment group, $p < 0.0001$ for both comparisons (Fig. 1B). While MC3 did have significantly higher transfection than the no treatment group ($p = 0.0411$), SM-102 LNPs was found to have the highest transfection *in vitro*. No significant differences were determined between treatment groups in metabolically active cells revealing no cytotoxic effects with any treatment, $F(2,6) = 0.6803$, $p = 0.5416$ (Fig. 1C).

3.2. SM-102 LNPs prolonged mRNA delivery in murine tibia fracture healing model

Due to the promising transfection kinetics seen *in vitro*, both LNP formulations were tested in our murine tibia fracture model to assess transfection efficacy and kinetics. Daily IVIS images were taken of all treatment groups (Fig. 2A) and the bioluminescence was quantified (Fig. 2B) within the standardized region of interest (ROI), $n = 3\text{-}5$. All IVIS output (total flux (p/s)) were log-transformed to normalize the total flux data. A two-way ANOVA revealed significant differences in luminescence between time points and treatment groups, $F(18, 97) = 5.441$, $p < 0.0001$. All further significance gained from Tukey's multiple comparison testing between the PBS control and either MC3 or SM-102 can be found on **FGURE 2A**. SM-102 LNPs had significantly more total flux than MC3 LNPs at day 2 after treatment ($p = 0.0463$), but no other differences were found between SM-102 and MC3 LNPs at any other day tested. The MC3 LNP group had significantly higher luminescence as compared with PBS controls on days 1–5 following injection, while SM-102 LNPs had significantly higher luminescence as compared to PBS at days 1–7 post-injection (Fig. 2A and B). SM-102 LNPs sustained transfection for 7 days following treatment as compared to MC3 LNPs which sustained transfection for 5 days. Further measures of transfection were taken as firefly luciferase RNA expression was quantified within the fracture callus (Fig. 2C). A two-way ANOVA revealed no significant differences in luciferase expression between time and treatment group, $F(2,16) = 1.021$, $p = 0.3826$. Although SM-102 LNPs trended with the highest luciferase activity 1 day after injection, this difference did not reach significance.

3.3. SM-102 LNPs do not alter localized inflammatory response or osteogenic gene expression within fracture callus

Local inflammatory response to the Luciferase mRNA-loaded LNPs was evaluated within the fracture callus using gene expression analysis, $n = 3\text{-}5$. A two-way ANOVA revealed no significant differences in *il-1β*

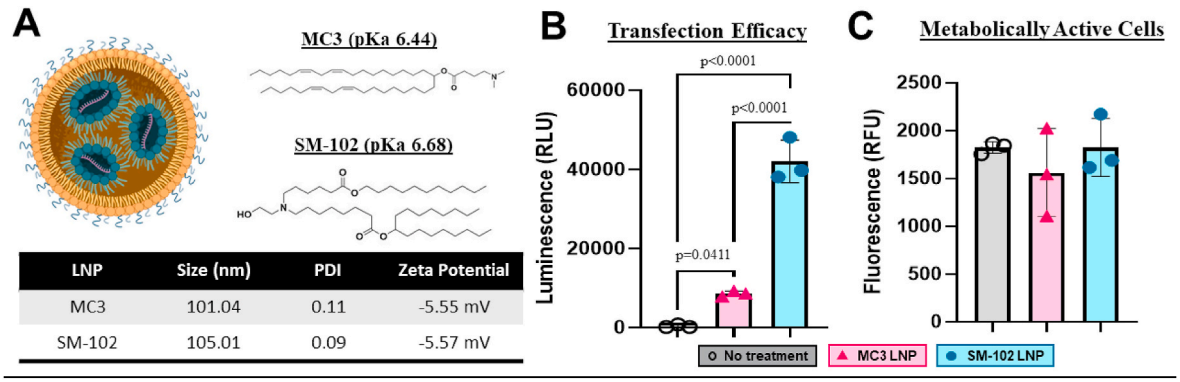

LNP	Size (nm)	PDI	Zeta Potential
MC3	101.04	0.11	-5.55 mV
SM-102	105.01	0.09	-5.57 mV

Fig. 1. Characterization of MC3 and SM-102 ionizable LNPs. **A).** Schematic representation of LNPs, structure of ionizable lipids SM-102 and MC3, and characteristics, **B).** transfection efficacy of firefly luciferase loaded LNPs, and **C).** metabolic activity of LNPs *in vitro*. Schematic created with Biorender.com.

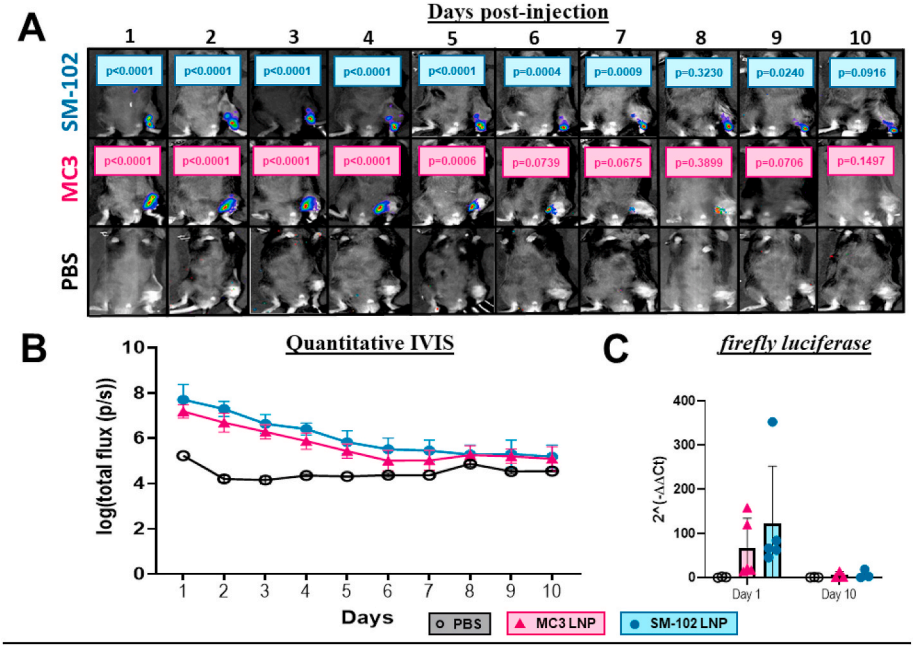

Fig. 2. A). Daily IVIS images after delivery of MC3 and SM-102 LNPs, and **B).** log-transformed quantitative IVIS. **C).** Firefly luciferase RNA expression was assessed within the fracture callus. All p-values listed on A represent the differences between either MC3 or SM-102 LNPs and the PBS control respective to each day.

expression between time and treatment group, $F(2,16) = 1.572$, $p = 0.2380$, but showed significant differences in tnf-α expression between time and treatments, $F(2,16) = 8.230$, $p = 0.0035$ (Fig. 3A and B). Tukey's multiple comparisons showed MC3 had significantly higher tnf-α expression at day 10 as compared to the PBS control and SM-102 LNPs ($p = 0.0393$, $p = 0.0009$ respectively).

To assess systemic inflammatory response from delivery of LNPs, C-reactive protein (CRP) was measured in the serum 1 and 10 days following treatments, $n = 3$-5 (Fig. 3C). A two-way ANOVA revealed significant differences in CRP activity between days and treatments, $F(2,10) = 9.364$, $p = 0.0051$. MC3 LNPs had the highest amount of CRP 1 day following treatment as compared with PBS and SM-102 from Tukey's multiple comparison analysis ($p < 0.0001$, $p = 0.0033$, respectively). Additionally, SM-102 had more CRP activity as compared to PBS control 1 day after treatment, $p = 0.0039$. No significant differences were found between treatment groups at 10 days after injection. To measure effect on fracture healing, the expression of osteogenic genes *Alp* and *Col10a1* were compared between groups, $n = 3$-5. No significant differences were determined in the expression of the early osteogenic marker *Alp* between days and treatment groups as revealed by a two-way ANOVA, $F(2,16) = 0.73$, $p = 0.4973$ (Fig. 3D). However, significant differences were found between treatments when testing *Col10a1* expression analyzing simple main effects, $F(2,16) = 8.972$, $p = 0.0024$. Sidak's multiple comparison's testing showed SM-102 at day 1 following injection to have significantly more *Col10a1* expression than MC3 LNPs, $p = 0.0149$ (Fig. 3E). No significant differences in *Col10a1* were found between the MC3 and PBS groups, nor SM-102 and PBS at any time point.

3.4. Biodistribution remained largely localized to the fracture site following LNP injection

A biodistribution study was performed to characterize the distribution of the LNPs following a localized injection to the site of the fracture callus, $n = 5$. It is important to determine if the LNPs remained localized or if they distribute through the reticuloendothelial system. All IVIS output (total flux (p/s)) were log-transformed to normalize and reduce the skewness of the total flux. A two-way ANOVA was performed to examine the effect of time and treatment group on luminescence. There was a statistically significant interaction between time and treatment group on luminescence, $F(2,10) = 39.98$, $p < 0.0001$, and all further significance gained from Tukey's multiple comparison testing is listed

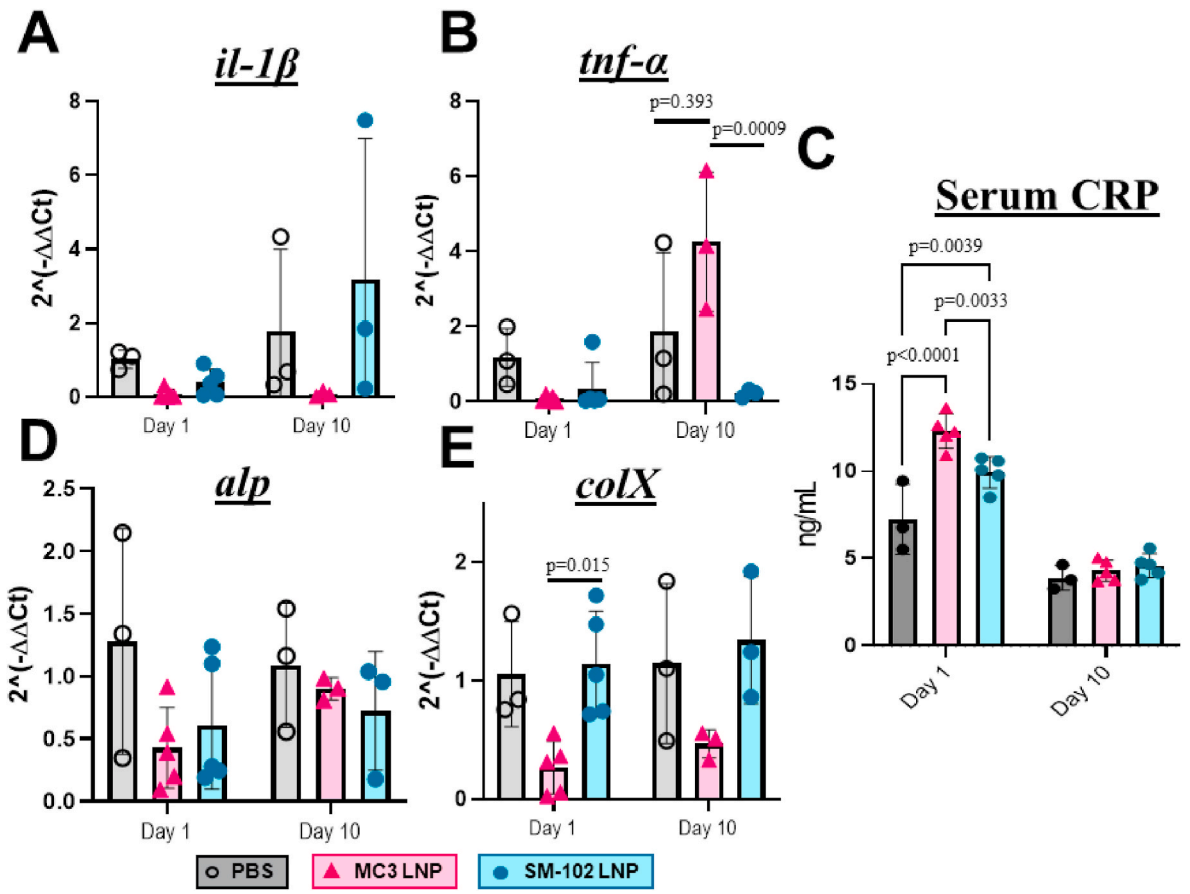

Fig. 3. Gene expression analysis of the fracture callus through qRT-PCR for markers of **A-B).** inflammation with il-1β and tnf-α, and **D-E).** osteogenesis with alkaline phosphatase and collagen 10a1 (colX). **C).** Additionally, C-reactive protein in serum was analyzed at days 1 and 10 after treatment.

on **FGURE 4A-C**. No significant differences were found between MC3 and SM-102 LNPs at 6 or 18 h ($p = 0.8073$ and $p = 0.575$ respectively). A two-way ANOVA was conducted to determine statistical significance in log-transformed total flux between main organs and tissues and treatment groups, $F(8,50) = 1.893$, $p = 0.082$. Pairwise comparisons revealed no significant differences were noted in luciferase expression between *ex-vivo* IVIS images of any of the groups tested in liver, lung, kidney or spleen tissues (Fig. 4B–D). However, MC3 and SM-102 had significantly higher luciferase signal in the fractured limbs when compared to the PBS control ($p = 0.0003$, $p = 0.0002$ respectively), but no significance was determined between the MC3 and SM-102 LNP groups ($p = 0.977$).

3.5. β-catenin^{GOF} mRNA activates canonical Wnt in vitro

To assess bioactivity of β-catenin^{GOF} mRNA, all groups were treated for 6 h prior to assessing downstream canonical Wnt markers and canonical Wnt reporter assay, Topflash, $n = 3$. An ordinary one-way ANOVA was conducted to determine statistical significance in relative gene expression for both *axin2* and *runx2* genes between the treatment groups, $F(2,6) = 209.1$, $p < 0.0001$ and $F(2,6) = 8.07$, $p = 0.0199$, respectively. *Axin2* expression was significantly higher in the rhWnt3a treated group as compared with the negative control ($p = 0.0003$), yet β-catenin^{GOF} mRNA showed the highest *axin2* expression over both rhWnt3a ($p < 0.0001$) and the negative control ($p < 0.0001$) (Fig. 5A). Additionally, β-catenin^{GOF} mRNA significantly increased *runx2* expression as compared with the negative control ($p = 0.212$), yet no significance was determined between β-catenin^{GOF} mRNA and rhWnt3a group ($p = 0.0513$) (Fig. 5B). Statistical significance in Topflash was determined from conducting an ordinary one-way ANOVA, $F(2,6) = 55.28$, $p = 0.0001$, revealing significance between firefly:renilla luciferase activity and treatment groups. Tukey's multiple comparisons testing revealed no significant differences in Wnt reporter assay, Topflash, between the β-catenin^{GOF} mRNA group and negative control ($p = 0.105$) despite β-catenin^{GOF} mRNA group trending higher (Fig. 5C). As expected, positive control rhWnt3a significantly enhanced Wnt activity as compared to both the negative control ($p = 0.0001$) and β-catenin^{GOF} mRNA group ($p = 0.0007$).

3.6. SM-102-β-catenin^{GOF} mRNA activates canonical Wnt and stimulates bone formation in vivo

SM-102-β-catenin^{GOF}mRNA was then tested histomorphometrically in its abilities to promote bone formation in a murine tibia fracture model. All tissues were harvested and analyzed at 2 weeks post-fracture, or 8 days post-SM-102- β-catenin^{GOF} mRNA treatment for all histological ($n = 7$-10), μCT ($n = 6$-8) and immunohistochemical evaluations ($n = 5$). A two-way ANOVA was conducted to determine significant differences in bone and cartilage composition between treatment groups, $F(4,54) = 13.55$, $p < 0.0001$. An ordinary one-way ANOVA was executed to determine significance in percent BV/TV between treatment groups, $F(4,35) = 3.608$, $p = 0.0145$. Multiple comparisons testing of histomorphometry data showed increased bone composition in the SM-102-β-catenin^{GOF} mRNA 45 μg group over the PBS control, $p = 0.0002$ (Fig. 7E and F). Additionally, SM-102-β-catenin^{GOF}mRNA 45 μg group had significantly more total bone area than the 10 μg/mouse group, $p = 0.0051$. The two higher concentrations of SM-102 β-catenin^{GOF}mRNA of 25 and 45 μg had significantly less cartilage composition within the fracture callus as compared to the PBS group ($p < 0.0001$ and $p = 0.0011$ respectively). The 25 μg group also had less cartilage composition than the 10 μg group ($p = 0.0036$). MicroCT quantification of bone

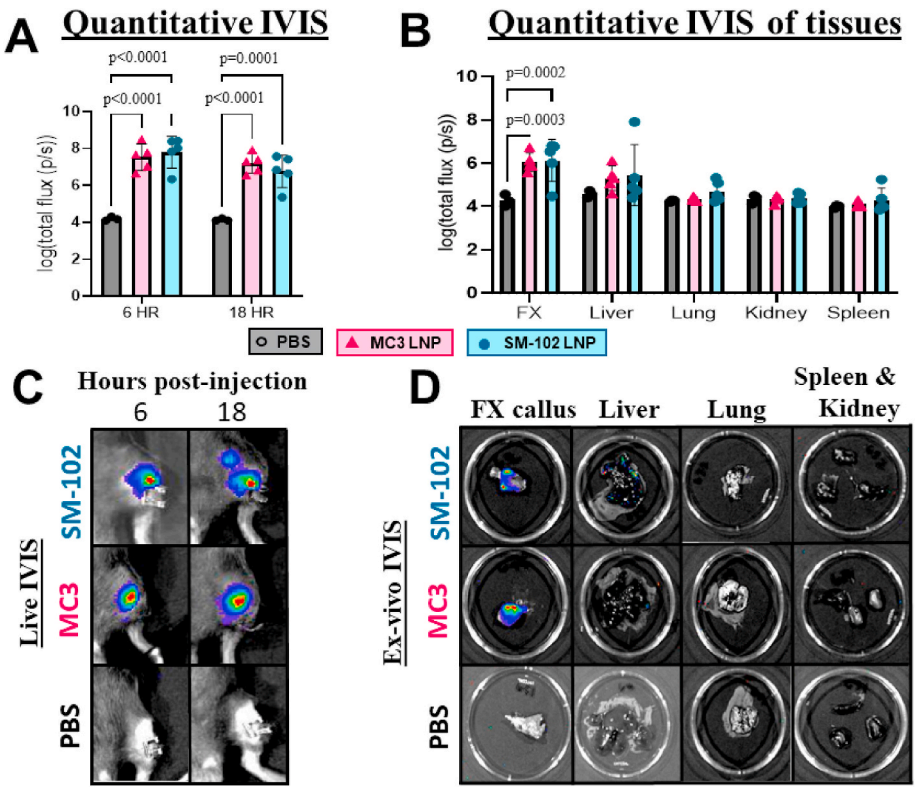

Fig. 4. Biodistribution study was performed to determine if the injections were localized to the fracture. **A,C).** Live IVIS imaging was performed at 6 and 18 h following injections and **B,D).** ex-vivo IVIS was performed on various organs and tissues.

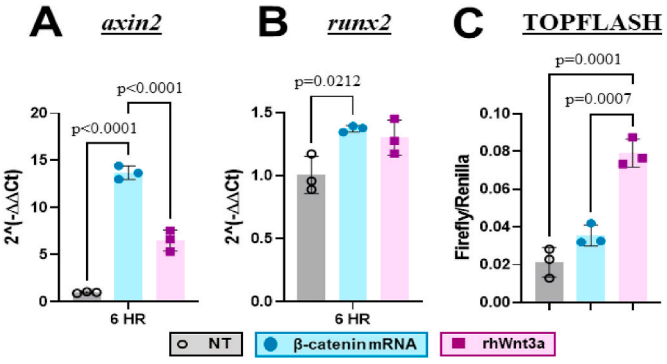

Fig. 5. Canonical Wnt bioactivity of β-catenin^{GOF}mRNA *in vitro* in a hypertrophic chondrocyte model. Specifically, **A).** genes downstream from canonical Wnt pathway were tested and **B).** a canonical Wnt reporter assay, Topflash.

was consistent with the histomorphometric results and showed significantly more bone volume following the delivery of SM-102-β-catenin^{GOF} mRNA 45 μg group compared to the PBS control ($p = 0.0328$) (Fig. 6 A, B). No significant differences were found in any of the other groups tested, or in any of the other measurements acquired (Fig. 6C).

Immunohistochemistry staining was performed using an anti-non-phosphorylated β-catenin antibody which detects activated form of β-catenin. The samples in the PBS group showed some positive stain suggesting endogenous expression in bone and in hypertrophic chondrocytes. The rhWnt3a samples showed positive β-catenin staining for all of the tissue types. The SM-102 β-catenin^{GOF} mRNA groups showed β-catenin expression with all doses tested and in bone and cartilage tissues within the callus (Fig. 8A–C). No β-catenin expression was observed in the negative control for the primary antibody in any group or tissue tested (Fig. 8D and E). These data taken together indicate that treatment with SM-102-β-catenin^{GOF} mRNA activates the canonical Wnt signaling pathway as detected in all main tissue types within a fracture callus.

4. Discussion

Therapeutic mRNA has shown great success with worldwide vaccination against COVID-19 using mRNA lipid nanoparticles [55–57]. However, the use of mRNA delivery to address musculoskeletal diseases, specifically for bone healing, remains a nascent field [58]. Expansion of this technology holds promise for regenerative medicine especially for healing of musculoskeletal diseases. Here, we demonstrate that local delivery of mRNA targeting canonical Wnt pathway delivered using SM-102 LNPs promoted bone *in vitro* and in our murine tibia fracture model. Most previous RNA-based therapeutic approaches for bone tissue regeneration have employed mRNA encoding bone morphogenetic proteins (BMPs) [59,60]. Elangovan et al. used a cationic polymer to complex with the negatively charged nucleic acid, termed polyplex, loaded onto a collagen scaffold and tested in a rat calvarial bone defect model [59]. It was reported that this chemically modified mRNA (cmRNA) encoding BMP-2 significantly increased bone volume as compared to the plasmid DNA polyplex encoding BMP-2 [59]. Other approaches using lipoplexes encapsulating cmBMP-2 have used various scaffolding materials including collagen sponge, poly-lactic-co-glycolic acid (PLGA) microparticles and also calcium phosphate cement to slow the release kinetics of the mRNA being delivered [61–64]. Importantly, all studies have reported therapeutic efficacy with incorporation of cmRNA encoding BMP-s *in vitro*, bone defect or integration models [59,61–64]. Despite the therapeutic benefits seen, all strategies have required surgical intervention to implement treatment. However, an injectable system that does not require surgical implantation would be ideal, as this would mitigate risks and healthcare costs associated with surgery [57,65–67].

In these experiments, two ionizable lipids were tested in LNP

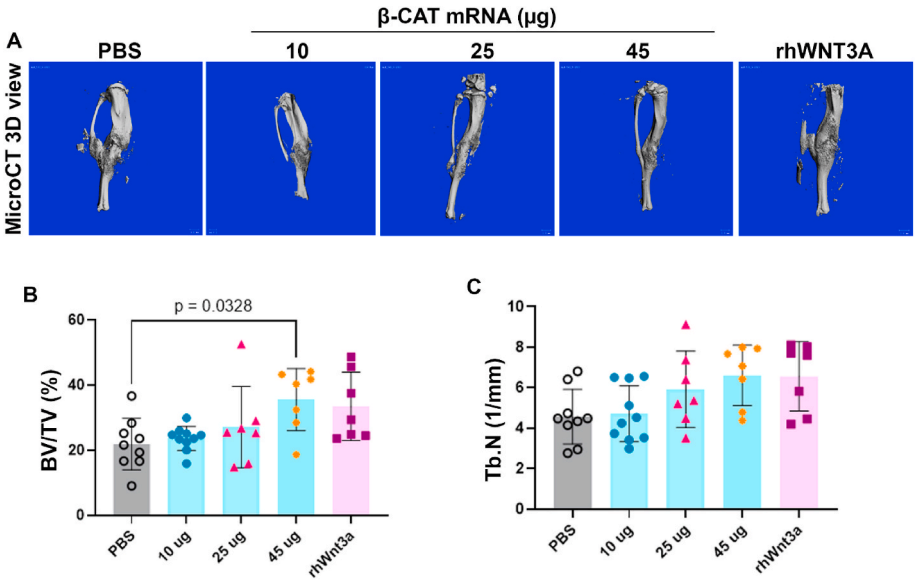

Fig. 6. MicroCT of all fractured tibias were evaluated for bone volume at 2 weeks after fracture. **A).** Representative 3D images of each treatment group. **B).** Percentage of bone volume over total volume and **C).** trabecular number were recorded for each sample tested.

formulations for fracture healing applications, with the goal of improving mRNA transfection efficiency, while assessing immunogenicity and biodistribution following localized injections. LNPs are comprised of naturally occurring components, like cholesterol, conferring them biocompatible and having a 'bioinspired' design [57]. Both MC3 LNPs and SM-102 LNPs were formulated with the same concentration of cholesterol, helper lipids, and pegylated lipids to ensure direct comparison of the two LNP formulations. Modifications to LNP composition are an innovative strategy used to tailor different aspects of LNP-based genetic cargo delivery, such as targeting and endosomal escape [70,71]. Here, given the importance of the apparent pK_a of the ionizable lipid depending on the type of genetic cargo, we compared a DLin-MC3-DMA-based control formulation (with the same composition of the Onpattro formulation for siRNA delivery) to a test formulation including SM-102 as ionizable lipid. In fact, changes in apparent pK_a from 6.44 (DLin-MC3-DMA) to 6.68 (SM-102) have been shown to be more suitable for mRNA delivery [32]. Additionally, we assessed improvements in cargo delivery between the control MC3 LNPs and SM-102 LNPs, which exploited DOPC as a helper lipid, instead of the typical DSPC. The design strategy for LNP lipid components revolves around their capacity to trigger non-bilayer (known as type H_{II}) lipid structures, essential for facilitating membrane fusion events that enable the intracellular delivery of macromolecules like mRNA [68]. It is widely acknowledged that unsaturated phospholipids, such as DOPC, exhibit strong compatibility with H_{II} structures [69–71]. In the case of DOPC, characterized by two unsaturated fatty acid tails of oleic acid, an expansion of the hydrophobic region leads to a molecular configuration that promotes membrane fusion and disruption of the bilayer. Hence, maintaining a substantial degree of chain unsaturation in the lipophilic region of a lipid bilayer plays a major role in destabilizing the intracellular bilayer of the endosome, therefore allowing the release of the cargo in the cytoplasm.

These observations are echoed by both our *in vitro* and *in vivo* results with luciferase mRNA. In fact, our *in vitro* investigation showed significantly increased transfection efficiency when treating chondrocytes with luciferase-loaded SM-102 LNPs, when compared to the MC3-based formulation. Additionally, SM-102 LNPs enabled signal detection *in vivo* for up to 8 days post-administration, when compared to only 6 days for the MC3 control formulation. Changes in the lipid composition of our test formulation did not affect LNP physio-chemical properties nor encapsulation efficiency, as both MC3 and SM-102 formulations showed similar stability in size, polydispersity index, Zeta potential, and encapsulation efficiency when evaluated after 28 days of storage at 4 °C. This clearly indicated that the use of an unsaturated helper lipid does not affect the overall structure of the LNP and that SM-102 LNPs improved delivery of mRNA by endosomal escape, facilitating greater endogenous protein expression.

Due to the promiscuity of LNPs seen following localized administration, it is imperative to examine the immunogenicity and biodistribution of these therapeutics. In our work, a localized injection within the fracture callus was selected to enhance site-specificity [72–74]. The SM-102-mRNA platform that was developed in this study has shown to present protein at biologically active levels for 8 days following treatment. In studies using similar mRNA gene therapeutics encapsulated by LNPs, such as the SARS-CoV-2 vaccine, protein expression was reported for 9 days near the injection site in preclinical models [75]. Despite using a localized route of administration, mRNA-based pharmaceuticals have been found to diffuse within circulation and thus provoke an immunogenic response [74]. While no cytotoxic effects were noted when testing either LNP formulation *in vitro,* MC3 LNPs were found to upregulate the pro-inflammatory factor TNFα within the fracture callus. While MC3 was the only formulation to provoke a localized immunogenic response, all injections including the control were shown to elevate systemic inflammatory factor, CRP, with MC3 formulation being the highest. Despite the elevated levels of inflammatory responses, no interference of osteogenesis was noted within the fracture callus with any formulation tested. Additionally, studies have shown that intramuscular injections of neutral, ionizable LNPs distribute to the liver, suggesting similar off-target risks [73]. In fact, Di et al. echoed this distribution profile and found greater lymphatic uptake with nanoparticles under 200 nm [76]. The detection of LNPs and cargo products in tissues other than the intended tissue necessitates assessment for safety and efficacy profiles. In this study, localized treatments of neutral LNPs did not show significant luciferase expression in liver, lung, spleen or kidney when tested *ex-vivo*. Given these results, mRNA delivery with SM-102 LNPs has the potential to promote a greater biological outcome in a fracture healing application while minimizing immunogenicity without interfering with osteogenesis.

Following the selection of the optimized LNP to deliver mRNA for fracture healing applications, we aimed to develop and validate a functional mRNA sequence encoding β-catenin to promote bone regeneration by activating the canonical Wnt signaling pathway. We

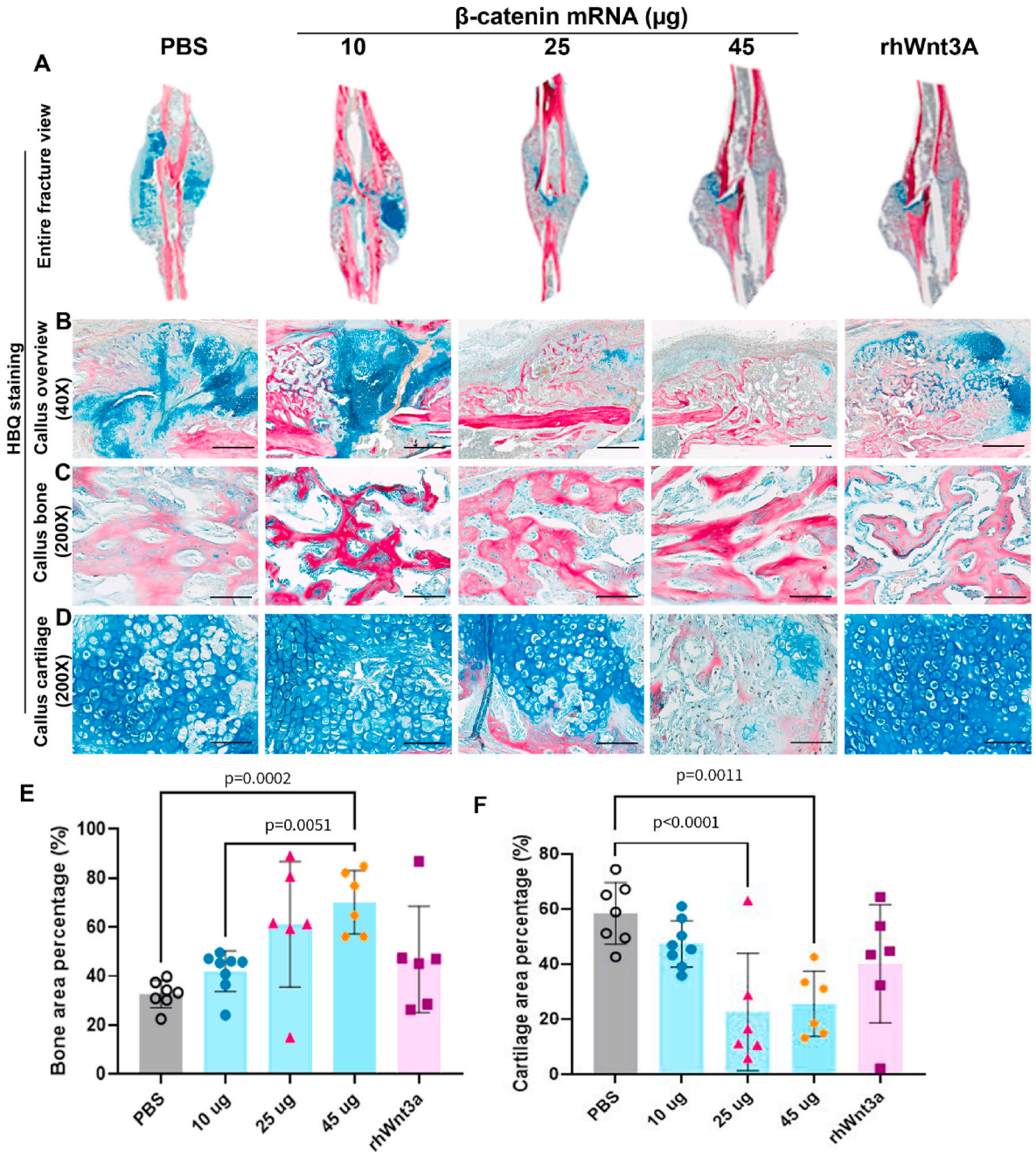

Fig. 7. Histomorphometry was performed to quantify bone and cartilage composition for all treatment groups 2 weeks after fracture. Representative images of each treatment group of **A).** the entire callus region (40X), **B).** an overview of the callus region (40X), **C).** newly formed trabecular bone (200X) and **D).** cartilage regions within the callus (200X). The regions were quantified using standard histomorphometric principles and the percent area of each region can be viewed in **E).** for bone and **F).** for cartilage. Scale bars at 40X magnification represent 500 μm and at 200X they represent 100 μm.

hypothesized that Wnt signaling activation during fracture repair was an ideal therapeutic target as an alternative to BMP, based on our discovery that this pathway plays a key role in the transformation of chondrocytes to osteoblast during the endochondral phase of fracture healing [11,18]. An in depth review on canonical Wnt for bone healing has previously been detailed in a review [77]. β-catenin was selected as the target mRNA sequence to activate the Wnt pathway and a mutant, stabilized β-catenin sequence was optimized to enhance β-catenin expression and protection from proteolytic destruction compared to wild-type β-catenin [33,78]. This constitutive stabilization of β-catenin, β-catenin^{GOF}, was proposed in this study to facilitate maximal β-catenin expression through the mRNA therapeutic, with potentially lower doses.

There has been limited research exploring RNA-based transcripts activating the canonical Wnt pathway to promote bone regeneration [60,79]. However, Zhang et al. aimed to activate canonical Wnt in a mandible bone repair application through co-delivery of vascular endothelial growth factor (VEGF) and Runx2 mRNA transcripts [80]. Here, mRNAs were delivered using polymeric nanomicelles in a rat mandibular bone defect model resulting in the most amount of bone regeneration with the co-delivered mRNAs [80]. While Runx2 does activate the canonical Wnt pathway, the direct interaction between these two regulators is not yet well established. However, both β-catenin and Runx2 play key roles in osteoblast proliferation and differentiation [81]. Interestingly, overexpression of Runx2 in mice resulted in an osteoporotic phenotype which was rescued by activation of canonical Wnt [81]. These results together suggest that activation of canonical

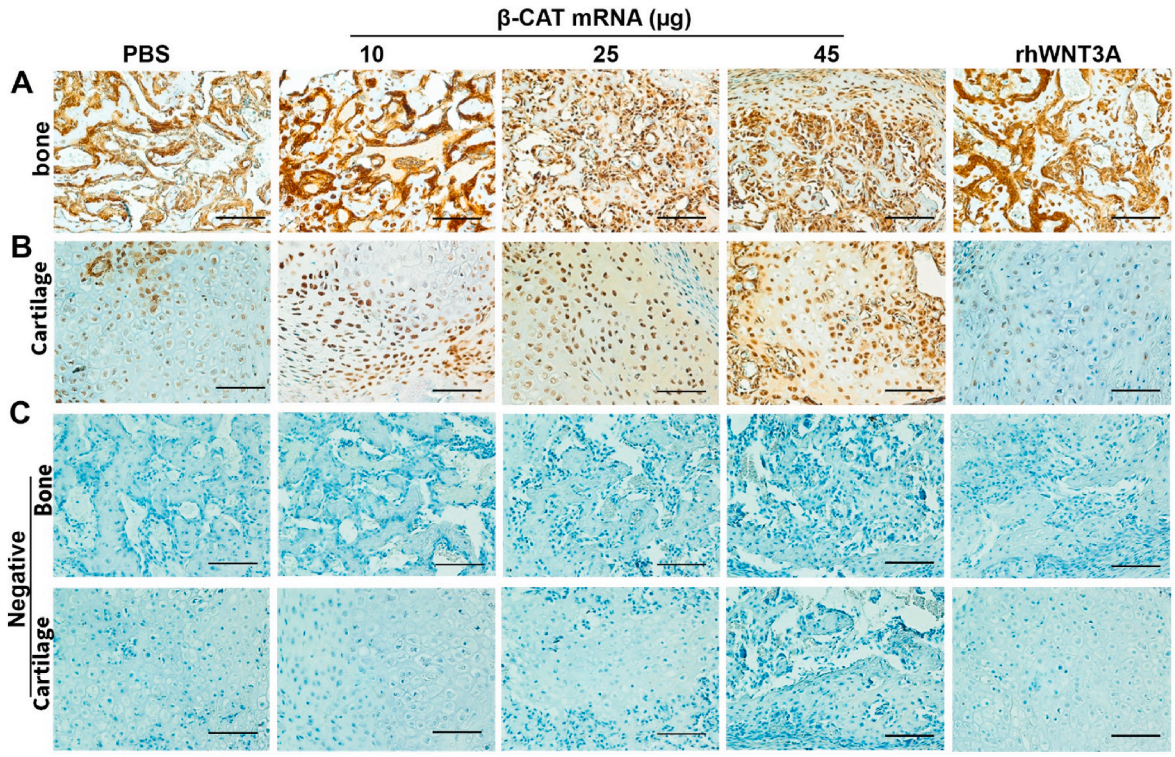

Fig. 8. Immunohistochemistry for β-catenin was employed to confirm β-catenin protein expression within tissues of the fracture callus including **A).** bone and **B).** cartilage tissues following treatments. **C).** Negative control entailed testing for non-specific antibody staining in both bone and cartilage tissues. Scale bars represent 100 μm.

Wnt is imperative in osteoblast proliferation and differentiation while Runx2 is heavily implicated in bone resorption and remodeling [82]. Thus, our approach which involves the direct activation of canonical Wnt, through delivery of β-catenin, and sequential modulation of Runx2 expression may be more effective for promoting bone in a fracture healing application [81].

Verification of canonical Wnt activation following delivery of SM-102-β-catenin^{GOF} mRNA was performed through gene expression analysis for *in vitro* testing and through immunohistochemistry for β-catenin for all *in vivo* studies. The developed therapeutic's bioactivity was confirmed as SM-102-β-catenin^{GOF} mRNA had higher *axin2* and *runx2* expression and stained positively for β-catenin *in vivo*. As interventions which stimulate osteoblast differentiation have the capacity to accelerate fracture healing, we next aimed to test capabilities of SM-102-β-catenin^{GOF} mRNA in stimulating bone formation *in vivo* [83]. Significantly more bone composition was determined in the 45 μg SM-102-β-catenin^{GOF} mRNA groups through histomorphometry. The only group which revealed significantly more bone in both histomorphometry and μCT was the 45 μg SM-102-β-catenin^{GOF} mRNA group, suggesting this dose may accelerate bone healing in our murine tibia fracture model. These sets of experiments together show that treatment with SM-102- β-catenin^{GOF} mRNA promotes chondrocytes within the fracture callus to express β-catenin, to upregulate canonical Wnt markers, *Axin2* and *Runx2* and ultimately to promote bone formation. Further, increased bone volume and bone composition imply that the SM-102-β-catenin^{GOF} mRNA therapeutic promotes chondrocytes to transdifferentiate into osteoblasts through activation of canonical Wnt signaling. Despite Wnt ligand rhWnt3a showing bioactivity *in vitro*, rhWnt3a was not found to be efficacious in stimulating bone *in vivo*. This data remains consistent with prior reports on the limited clinical efficacy of relatively insoluble rhWnt3a [84,85]. In conclusion, the mRNA therapeutic described in this study can overcome limitations seen with other mRNA platforms for bone regeneration which require surgical intervention and the gain of function sequence has the potential to minimize the therapeutic dose.

Despite the novelty of these findings, there are several challenges that need further exploration and remain as potential limitations in our approach. One main limitation is that all immunogenicity, fracture interference and biodistribution studies were performed following a single concentration of mRNA. Delivery with higher mRNA concentrations may only heighten the innate immune reaction as mRNA delivery activates the cell's antiviral defense mechanism through production of type I interferons and pro-inflammatory cytokines [86–89]. Thus, future studies should address the use of higher mRNA concentrations on localized and systemic immune responses. In addition to immunogenicity, biodistribution should be re-evaluated with increased concentrations. While no significant luciferase expression levels were found when in the liver after a localized delivery of 10 μg/mouse, a nearly five-fold increased dose may show a varied distribution profile.

Effective mRNA delivery to cells requires the use of carriers that will protect the nucleic acids from degradation from nucleases [90,91]. Currently, liposomal complexes (lipoplexes) are the most commonly utilized delivery vehicles for mRNA based therapeutics, and include lipid nanoparticles and liposomes [90,91]. However, lipoplexes can induce immunogenic reactions and are rapidly cleared by the mononuclear phagocytic system (MPS) [90]. Alternative strategies have been employed to mitigate limitations seen with liposomal delivery and to effectively transport genes for bone repair, including the use of β-tricalcium phosphate biomaterials and mineral coated microparticles (MCM) [92–94]. Although the majority of publications focus on MCMs to deliver proteins in a controlled-release manner, recent work has focused on the controlled release dynamics of lipoplexes using MCMs [94–96]. However these approaches have yet to be translated into the clinic.

Future work entails establishing the full time course of fracture repair and remodeling, as the current work was limited by testing only one time point at 2 weeks following fracture. The long-term effects of this novel therapy are important to test as aberrant bone growth has

been reported to occur in mice at 4 months following treatment with BMP-2 [97]. Further, to confirm that SM-102-β-catenin^{GOF} mRNA accelerates fracture healing, longer time points need to be assessed through uCT and histomorphometry. Specifically, for this model, additional time points at 4 and 6 weeks after fracture would sufficiently determine earlier healing.

5. Conclusions

In summary, we have developed an injectable and biocompatible method to deliver functional mRNA modalities specifically for bone tissue regeneration. SM-102-β-catenin^{GOF} mRNA was found to increase bone formation in a murine tibia fracture model, indicating its potential to be used to accelerate fracture healing. Given the high number of delayed or non-union fractures, this approach has the potential for significant clinical impact and deserves further development. Given the potential of injectable SM-102-β-catenin^{GOF} mRNA to accelerate fracture healing without requiring additional surgeries, this therapeutic may have the capacity to reduce healthcare costs and morbidity associated with impaired fracture healing.

Ethics approval and consent to participate

All In vivo experiments were approved by and conducted in compliance with the Institutional Animal Care and Use Committee at Colorado State University (CSU) under protocol number 4575.

CRediT authorship contribution statement

Anna Laura Nelson: Writing – review & editing, Writing – original draft, Methodology, Investigation, Funding acquisition, Formal analysis, Data curation, Conceptualization. **Chiara Mancino:** Writing – review & editing, Writing – original draft, Methodology, Formal analysis, Data curation, Conceptualization. **Xueqin Gao:** Formal analysis, Data curation. **Joshua A. Choe:** Writing – review & editing, Methodology, Data curation. **Laura Chubb:** Writing – review & editing, Methodology, Data curation. **Katherine Williams:** Writing – review & editing, Data curation. **Molly Czachor:** Data curation. **Ralph Marcucio:** Writing – review & editing, Methodology, Conceptualization. **Francesca Taraballi:** Writing – review & editing, Resources, Methodology, Investigation, Conceptualization. **John P. Cooke:** Writing – review & editing, Supervision, Resources, Project administration, Methodology, Conceptualization. **Johnny Huard:** Writing – review & editing, Resources, Project administration, Investigation, Funding acquisition. **Chelsea Bahney:** Writing – review & editing, Supervision, Resources, Methodology, Investigation, Funding acquisition, Conceptualization. **Nicole Ehrhart:** Writing – review & editing, Supervision, Resources, Methodology, Investigation, Funding acquisition, Conceptualization.

Declaration of competing interest

Anna Laura Nelson, Chiara Mancino, Xueqin Gao, Josh Choe, Laura Chubb, Katherine Williams, Molly Czachor, Ralph Marcucio and Francesca Taraballi have nothing to disclose. Dr. Johnny Huard discloses an unpaid position on the leadership for Orthopaedic Research Society (ORS). JH discloses royalties from Cook Myosite, Inc. Dr. Cooke is on the Scientific Advisory Board of Humann Inc, which makes products related to nitric oxide and cardiovascular health; is an inventor on multiple patents assigned to Stanford University or Houston Methodist Hospital related to endothelial function and regeneration; and has been a collaborator and co-author with Dr. Zhen Chen. Dr. Chelsea Bahney discloses an unpaid position on the leadership for Orthopaedic Research Society (ORS), Tissue Engineering and Regenerative Medicine International Society (TERMIS), and the Orthopaedic Trauma Association (OTA). CB also discloses IP royalties from Iota Biosciences, Inc. for US Patent 041263 and a Review Editor role for Frontiers in Skeletal Physiology. Dr. Nicole Ehrhart discloses paid consultant positions for Onkos Surgical Inc. and Ripple Neuromed Inc. ALN, CM, JH, RM, JCooke, FT, CB, NE also disclose inventorship on PCT/US2022 Application No. 63/155,263, entitled *MCM For Gene Therapy to Activate Wnt Pathway*. **These entities provided no funding for this research and there are no conflicts of interest with the work presented in this manuscript.**

Anna Laura Nelson, Dr. Johnny Huard, Dr. Xueqin Gao, Molly Czachor and Dr. Chelsea Bahney are all paid employees of the non-profit Steadman Philippon Research Institute (SPRI). SPRI exercises special care to identify any financial interests or relationships related to research conducted here. During the past calendar year, SPRI has received grant funding or in-kind donations from Arthrex, DJO, MLB, Ossur, Siemens, Smith & Nephew, XTRE, and philanthropy. These funding sources provided no support for the work presented in this manuscript unless otherwise noted.

Acknowledgements

Research reported in this publication was supported by National Institute of Arthritis and Musculoskeletal and Skin Diseases (NIAMS) of the National Institutes of Health (NIH) under award number R01 AR077761. We also gratefully acknowledge philanthropic support from the Musculoskeletal Regeneration Partnership Fund by Mary Sue and Michael Shannon and by Project Number 20–166 from the Orthoregeneration Network for Kick-Starter Grant. This work was supported by the National Institute on Aging of the National Institutes of Health under Award Number F30AG077748 and the University of Wisconsin – Madison Medical Scientist Training Program: T32GM140935. All content is solely the responsibility of the authors and does not represent the official views of National Institutes of Health, Orthoregeneration Network or Shannon Foundation. We thank Suzanne Page for her critical role in grant management and SPRI operations. All graphics were created with BioRender.com.

Appendix A. Supplementary data

Supplementary data to this article can be found online at https://doi.org/10.1016/j.bioactmat.2024.05.020.

References

[1] C.L. Ekegren, et al., Incidence, costs and predictors of non-union, delayed union and mal-union following long bone fracture, Int. J. Environ. Res. Publ. Health 15 (12) (2018).
[2] J.A. Cauley, The global burden of fractures, Lancet Healthy Longev 2 (9) (2021) e535–e536.
[3] R.J. Weiss, et al., Decreasing incidence of tibial shaft fractures between 1998 and 2004: information based on 10,627 Swedish inpatients, Acta Orthop. 79 (4) (2008) 526–533.
[4] C.M. Court-Brown, B. Caesar, Epidemiology of adult fractures: a review, Injury 37 (8) (2006) 691–697.
[5] K. Fong, et al., Predictors of nonunion and reoperation in patients with fractures of the tibia: an observational study, BMC Muscoskel. Disord. 14 (1) (2013) 103.
[6] A. Karladani, et al., The influence of fracture etiology and type on fracture healing: a review of 104 consecutive tibial shaft fractures, Arch. Orthop. Trauma Surg. 121 (2001) 325–328.
[7] R. Mundi, et al., Nonunion in patients with tibial shaft fractures: is early physical status associated with fracture healing? Cureus 12 (4) (2020).
[8] M.R. Brinker, et al., The devastating effects of tibial nonunion on health-related quality of life, J Bone Joint Surg Am 95 (24) (2013) 2170–2176.
[9] M. Panteli, et al., Biological and molecular profile of fracture non-union tissue: a systematic review and an update on current insights, J. Cell Mol. Med. 26 (3) (2022) 601–623.
[10] C.S. Bahney, et al., Cellular biology of fracture healing, J. Orthop. Res. 37 (1) (2019) 35–50.
[11] S.A. Wong, et al., Beta-catenin signaling regulates cell fate decisions at the transition zone of the chondro-osseous junction during fracture healing, bioRxiv (2020).
[12] R. Marcucio, T. Miclau III, C. Bahney, A shifting paradigm: transformation of cartilage to bone during bone repair, J. Dent. Res. 102 (1) (2023) 13–20.
[13] K.R. Garrison, et al., Bone morphogenetic protein (BMP) for fracture healing in adults, Cochrane Database Syst. Rev. (6) (2010).

[14] C.S. Bahney, et al., Cellular biology of fracture healing, J. Orthop. Res. 37 (1) (2019) 35–50.
[15] D.P. Hu, et al., Cartilage to bone transformation during fracture healing is coordinated by the invading vasculature and induction of the core pluripotency genes, Development 144 (2) (2017) 221–234.
[16] J. Kodama, et al., The role of hypertrophic chondrocytes in regulation of the cartilage-to-bone transition in fracture healing, BoneKEy Rep. (2022) 101616.
[17] C.S. Bahney, et al., Stem cell–derived endochondral cartilage stimulates bone healing by tissue transformation, J. Bone Miner. Res. 29 (5) (2014) 1269–1282.
[18] S.A. Wong, et al., β-Catenin signaling regulates cell fate decisions at the transition zone of the chondro-osseous junction during fracture healing, bioRxiv (2020), 2020.03.11.986141.
[19] I. Dumic-Cule, et al., Bone morphogenetic proteins in fracture repair, Int. Orthop. 42 (11) (2018) 2619–2626.
[20] K. Tsuji, et al., BMP2 activity, although dispensable for bone formation, is required for the initiation of fracture healing, Nat. Genet. 38 (12) (2006) 1424–1429.
[21] K.R. Garrison, I. S, S. Donell, J.J. Ryder, M. Mugford, I. Harvey, F. Song, Bone morphogenetic protein (BMP) for fracture healing in adults, Cochrane Database ofSystematic Reviews (1) (2008).
[22] S.N. Lissenberg-Thunnissen, et al., Use and efficacy of bone morphogenetic proteins in fracture healing, Int. Orthop. 35 (9) (2011) 1271–1280.
[23] C.E. Gillman, A.C. Jayasuriya, FDA-approved bone grafts and bone graft substitute devices in bone regeneration, Mater. Sci. Eng., C 130 (2021) 112466.
[24] S.N. Lissenberg-Thunnissen, et al., Use and efficacy of bone morphogenetic proteins in fracture healing, Int. Orthop. 35 (2011) 1271–1280.
[25] K.M. Cadigan, Y.I. Liu, Wnt signaling: complexity at the surface, J. Cell Sci. 119 (Pt 3) (2006) 395–402.
[26] R. Baron, G. Rawadi, Targeting the Wnt/beta-catenin pathway to regulate bone formation in the adult skeleton, Endocrinology 148 (6) (2007) 2635–2643.
[27] N. Krishnamurthy, R. Kurzrock, Targeting the Wnt/beta-catenin pathway in cancer: update on effectors and inhibitors, Cancer Treat Rev. 62 (2018) 50–60.
[28] M. Bhandari, et al., Romosozumab in skeletally mature adults with a fresh unilateral tibial diaphyseal fracture: a randomized phase-2 study, J Bone Joint Surg Am 102 (16) (2020) 1416–1426.
[29] T.R. Damase, et al., The limitless future of RNA therapeutics, Front. Bioeng. Biotechnol. 9 (2021) 628137.
[30] A. Akinc, et al., The Onpattro story and the clinical translation of nanomedicines containing nucleic acid-based drugs, Nat. Nanotechnol. 14 (12) (2019) 1084–1087.
[31] S. Qin, et al., mRNA-based therapeutics: powerful and versatile tools to combat diseases, Signal Transduct. Targeted Ther. 7 (1) (2022) 166.
[32] C.H. Albertsen, et al., The role of lipid components in lipid nanoparticles for vaccines and gene therapy, Adv. Drug Deliv. Rev. 188 (2022) 114416.
[33] N. Harada, et al., Intestinal polyposis in mice with a dominant stable mutation of the beta-catenin gene, EMBO J. 18 (21) (1999) 5931–5942.
[34] D. Adams, et al., Patisiran, an RNAi therapeutic, for hereditary transthyretin amyloidosis, N. Engl. J. Med. 379 (1) (2018) 11–21.
[35] Y. Gong, et al., R-spondin 2 induces odontogenic differentiation of dental pulp stem/progenitor cells via regulation of Wnt/β-catenin signaling, Front. Physiol. 11 (2020) 918.
[36] Y. Hwang, et al., WNT3A promotes myogenesis of human embryonic stem cells and enhances in vivo engraftment, Sci. Rep. 4 (2014) 5916.
[37] C. Caetano da Silva, et al., WNT11, a new gene associated with early onset osteoporosis, is required for osteoblastogenesis, Hum. Mol. Genet. 31 (10) (2022) 1622–1634.
[38] R. Gedaly, et al., Targeting the Wnt/β-catenin signaling pathway in liver cancer stem cells and hepatocellular carcinoma cell lines with FH535, PLoS One 9 (6) (2014) e99272.
[39] J. Kim, et al., Ubiquitin-specific peptidase 2a (USP2a) deubiquitinates and stabilizes β-catenin, Am. J. Cancer Res. 8 (9) (2018) 1823–1836.
[40] S.A. Wong, et al., β-catenin signaling regulates cell fate decisions at the transition zone of the chondro-osseous junction during fracture healing, bioRxiv (2020), 2020.03. 11.986141.
[41] T. Chen, et al., A WNT protein therapeutic improves the bone-forming capacity of autografts from aged animals, Sci. Rep. 8 (1) (2018) 119.
[42] A. Popelut, et al., The acceleration of implant osseointegration by liposomal Wnt3a, Biomaterials 31 (35) (2010) 9173–9181.
[43] A.I. Pogue, et al., Systemic inflammation in C57BL/6J mice receiving dietary aluminum sulfate; up-regulation of the pro-inflammatory cytokines IL-6 and TNFα, C-reactive protein (CRP) and miRNA-146a in blood serum, J Alzheimers Dis Parkinsonism 7 (6) (2017).
[44] K.O. Rivera, et al., Localized delivery of β-NGF via injectable microrods accelerates endochondral fracture repair, bioRxiv (2021), 2021.11.16.468864.
[45] B.K. Hall, The role of movement and tissue interactions in the development and growth of bone and secondary cartilage in the clavicle of the embryonic chick, J. Embryol. exp. Morph. 93 (1986) 133–152.
[46] D. Malhan, et al., An optimized approach to perform bone histomorphometry, Front. Endocrinol. 9 (2018).
[47] M.L. Bouxsein, et al., Guidelines for assessment of bone microstructure in rodents using micro–computed tomography, J. Bone Miner. Res. 25 (7) (2010) 1468–1486.
[48] X. Sun, et al., High bone microarchitecture, strength, and resistance to bone loss in MRL/MpJ mice correlates with activation of different signaling pathways and systemic factors, Faseb. J. 34 (1) (2020) 789–806.
[49] X. Gao, et al., The use of heparin/polycation coacervate sustain release system to compare the bone regenerative potentials of 5 BMPs using a critical sized calvarial bone defect model, Biomaterials 288 (2022) 121708.
[50] X. Gao, et al., Influences of donor and host age on human muscle-derived stem cell-mediated bone regeneration, Stem Cell Res. Ther. 9 (1) (2018) 316.
[51] X. Gao, et al., MRL/MpJ mice resist to age-related and long-term ovariectomy-induced bone loss: implications for bone regeneration and repair, Int. J. Mol. Sci. 24 (3) (2023).
[52] M. Danaei, et al., Impact of particle size and polydispersity index on the clinical applications of lipidic nanocarrier systems, Pharmaceutics 10 (2) (2018).
[53] J.D. Clogston, A.K. Patri, Zeta potential measurement, Characterization of nanoparticles intended for drug delivery (2011) 63–70.
[54] C. Mancino, et al., Harnessing RNA technology to advance therapeutic vaccine antigens against chagas disease, ACS Appl. Mater. Interfaces (2024).
[55] S.A. Meo, et al., COVID-19 vaccines: comparison of biological, pharmacological characteristics and adverse effects of Pfizer/BioNTech and Moderna Vaccines, Eur. Rev. Med. Pharmacol. Sci. 25 (3) (2021) 1663–1669.
[56] N. Al Kaabi, et al., Effect of 2 inactivated SARS-CoV-2 vaccines on symptomatic COVID-19 infection in adults: a randomized clinical trial, JAMA 326 (1) (2021) 35–45.
[57] A.-C. Burduşel, E. Andronescu, Lipid nanoparticles and liposomes for bone diseases treatment, Biomedicines 10 (12) (2022) 3158.
[58] R.E. De la Vega, et al., Gene therapy for bone healing: lessons learned and new approaches, Transl. Res. 236 (2021) 1–16.
[59] S. Elangovan, et al., Chemically modified RNA activated matrices enhance bone regeneration, J. Contr. Release 218 (2015) 22–28.
[60] A.K. Rajendran, S. Amirthalingam, N.S. Hwang, A brief review of mRNA therapeutics and delivery for bone tissue engineering, RSC Adv. 12 (15) (2022) 8889–8900.
[61] E.R. Balmayor, et al., Chemically modified RNA induces osteogenesis of stem cells and human tissue explants as well as accelerates bone healing in rats, Biomaterials 87 (2016) 131–146.
[62] M. Utzinger, et al., cmRNA/lipoplex encapsulation in PLGA microspheres enables transfection via calcium phosphate cement (CPC)/PLGA composites, J. Contr. Release 249 (2017) 143–149.
[63] W. Zhang, et al., An improved, chemically modified RNA encoding BMP-2 enhances osteogenesis in vitro and in vivo, Tissue Eng. 25 (1–2) (2019) 131–144.
[64] B. Khorsand, et al., A comparative study of the bone regenerative effect of chemically modified RNA encoding BMP-2 or BMP-9, AAPS J. 19 (2) (2017) 438–446.
[65] L. Zhou, et al., Bone-targeting liposome-encapsulated salvianic acid a improves nonunion healing through the regulation of HDAC3-mediated endochondral ossification, Drug Des. Dev. Ther. (2020) 3519–3533.
[66] De La Vega, R.E., et al., Efficient healing of large osseous segmental defects using optimized chemically modified messenger RNA encoding BMP-2. Sci. Adv.. 8(7): p. eabl6242..
[67] B. Wei, et al., Gelatin methacrylate hydrogel scaffold carrying resveratrol-loaded solid lipid nanoparticles for enhancement of osteogenic differentiation of BMSCs and effective bone regeneration, Regenerative Biomaterials 8 (5) (2021) rbab044.
[68] J.A. Kulkarni, P.R. Cullis, R. van der Meel, Lipid nanoparticles enabling gene therapies: from concepts to clinical utility, Nucleic Acid Therapeut. 28 (3) (2018) 146–157.
[69] E. Álvarez-Benedicto, et al., Optimization of phospholipid chemistry for improved lipid nanoparticle (LNP) delivery of messenger RNA (mRNA), Biomater. Sci. 10 (2) (2022) 549–559.
[70] X. Cheng, R.J. Lee, The role of helper lipids in lipid nanoparticles (LNPs) designed for oligonucleotide delivery, Adv. Drug Deliv. Rev. 99 (2016) 129–137.
[71] C. Lotter, et al., Incorporation of phosphatidylserine improves efficiency of lipid based gene delivery systems, Eur. J. Pharm. Biopharm. 172 (2022) 134–143.
[72] M.J. Carrasco, et al., Ionization and structural properties of mRNA lipid nanoparticles influence expression in intramuscular and intravascular administration, Commun. Biol. 4 (1) (2021) 956.
[73] K.J. Hassett, et al., Optimization of lipid nanoparticles for intramuscular administration of mRNA vaccines, Mol. Ther. Nucleic Acids 15 (2019) 1–11.
[74] X. Xu, T. Xia, Recent advances in site-specific lipid nanoparticles for mRNA delivery, ACS Nanosci Au 3 (3) (2023) 192–203.
[75] A.J. Krauson, et al., Duration of SARS-CoV-2 mRNA vaccine persistence and factors associated with cardiac involvement in recently vaccinated patients, npj Vaccines 8 (1) (2023) 141.
[76] J. Di, et al., Biodistribution and non-linear gene expression of mRNA LNPs affected by delivery route and particle size, Pharm. Res. (N. Y.) 39 (1) (2022) 105–114.
[77] A.L. Nelson, et al., Therapeutic approaches to activate the canonical Wnt pathway for bone regeneration, Journal of Tissue Engineering and Regenerative Medicine 16 (11) (2022) 961–976.
[78] S.H. Vijaya Chandra, et al., A common role for various human truncated adenomatous polyposis coli isoforms in the control of beta-catenin activity and cell proliferation, PLoS One 7 (4) (2012) e34479.
[79] S. Uchida, et al., mRNA as a tool for gene transfection in 3D cell culture for future regenerative therapy, Micromachines 11 (4) (2020) 426.
[80] M. Zhang, et al., Enhancement of bone regeneration by coadministration of angiogenic and osteogenic factors using messenger RNA, Inflamm. Regen. 43 (1) (2023) 32.
[81] C. Haxaire, E. Haÿ, V. Geoffroy, Runx2 controls bone resorption through the down-regulation of the Wnt pathway in osteoblasts, Am. J. Pathol. 186 (6) (2016) 1598–1609.
[82] Y. Wu, J. Han, S. Wen, Mechanism of Runx2 gene in fracture healing, Chinese Journal of Tissue Engineering Research 25 (14) (2021) 2274.
[83] P. Aspenberg, Special Review: accelerating fracture repair in humans: a reading of old experiments and recent clinical trials, BoneKEy Rep. 2 (2013) 244.

[84] G.R. Dhamdhere, et al., Drugging a stem cell compartment using Wnt3a protein as a therapeutic, PLoS One 9 (1) (2014) e83650.
[85] E. Mihara, et al., Active and water-soluble form of lipidated Wnt protein is maintained by a serum glycoprotein afamin/α-albumin, Elife 5 (2016).
[86] C. Pollard, et al., Type I IFN counteracts the induction of antigen-specific immune responses by lipid-based delivery of mRNA vaccines, Mol. Ther. 21 (1) (2013) 251–259.
[87] A. De Beuckelaer, et al., Type I interferons interfere with the capacity of mRNA lipoplex vaccines to elicit cytolytic T cell responses, Mol. Ther. 24 (11) (2016) 2012–2020.
[88] S. Linares-Fernández, et al., Tailoring mRNA vaccine to balance innate/adaptive immune response, Trends Mol. Med. 26 (3) (2020) 311–323.
[89] L. Sun, S. Liu, Z.J. Chen, SnapShot: pathways of antiviral innate immunity, Cell 140 (3) (2010) 436–436.e2.
[90] P.S. Kowalski, et al., Delivering the messenger: advances in technologies for therapeutic mRNA delivery, Mol. Ther. 27 (4) (2019) 710–728.
[91] J. Wei Nitika, A.M. Hui, The delivery of mRNA vaccines for therapeutics, Life 12 (8) (2022).
[92] R. Alluri, et al., Regional gene therapy with 3D printed scaffolds to heal critical sized bone defects in a rat model, J. Biomed. Mater. Res. 107 (10) (2019) 2174–2182.
[93] H.P. Kang, et al., Regional gene therapy for bone healing using a 3D printed scaffold in a rat femoral defect model, J. Biomed. Mater. Res. 109 (11) (2021) 2346–2356.
[94] G. Fontana, et al., Mineral-coated microparticles enhance mRNA-based transfection of human bone marrow cells, Mol. Ther. Nucleic Acids 18 (2019) 455–464.
[95] H. Martin, et al., 1127 Calcium Phosphate Biomaterials Enhance Immunotherapeutic mRNA Delivery in Melanoma, BMJ Specialist Journals, 2022.
[96] A.L. Nelson, et al., Mineral coated microparticles doped with fluoride and complexed with mRNA prolong transfection in fracture healing, Front. Bioeng. Biotechnol. 11 (2023) 1295313.
[97] B. Prados, et al., Heterotopic ossification in mice overexpressing Bmp2 in Tie2+ lineages, Cell Death Dis. 12 (8) (2021) 729.